Journal
of
Engineering and Technology
Vol. 1 No. 2 July- December 2002

Contents

Editorial iii

THE EFFECT OF CONVECTIVE HEAT TRANSFER COEFFICIENTS ON THE DESIGN OF CONDENSER AND EVAPORATOR OF A REFRIGERATION SYSTEM 01

A. K. M. Iqbal Hussain

A MODIFIED DIGITAL SIGNATURE STANDARD (DSS) ALGORITHM TO IMPROVE NETWORK SECURITY 11

Omer Ali Beshir, Elyas Towhid Sheik Mahmoud, Shareeful Islam

IMAGE TEXTURE CLASSIFICATION USING CORTEX TRANSFORM: A BLOCK PROCESSING APPROACH (BPA) 17

M. K. Bashar M. S. Islam N. Ohnishi

COMPARISON OF BUILT-IN-STORAGE AND NATURAL FLOW TYPE SOLAR WATER HEATERS 27

M. R. Alam, M. R. Rahaman, S. M. N. Shams, M. F. Ilahi , M. A. R. Akhanda

Islamic University of Technology (IUT)
The Organisation of Islamic Conference (OIC)
Board Bazar, Gazipur 1704, Bangladesh
Telephone: 880-2-9800960, 9800962, Fax : 880-2- 9800970
E-Mail: vc@iut-dhaka.edu Web: www.iutoic-dhaka.edu

Production: Europa, Bangladesh

IUT Journal of Engineering and Technology Vol. 1 No. 2 July - December 2002

بسم الله الرحمن الرحيم

Journal
of
Engineering and Technology
Vol. 1 No. 2 July - December 2002

الجامعة الاسلامية للتكنولوجيا
مخظمة المؤتمر الاسلامي

UNIVERSITE ISLAMIQUE DE TECHNOLOGIE (UIT)
L'ORGANISATION DE LA CONFERENCE ISLAMIQUE

ISLAMIC UNIVERSITY OF TECHNOLOGY (IUT)
THE ORGANISATION OF THE ISLAMIC CONFERENCE (OIC)

IMAGE TEXTURE CLASSIFICATION USING CORTEX TRANSFORM: A BLOCK PROCESSING APPROACH (BPA)

M. K. Bashar*, M. S. Islam, N. Ohnishi***

Abstract

We present a block-based multi-channel mechanism for image texture classification inspired by human visual system(HVS). The proposed approach compresses the feature space by adopting the filters within a small sliding block of data meaningful to relatively accurate boundary extraction. In our efforts, 2D Gaussian functions were used as bandpass cortex filters to simualte the behaviour of simple cells in HVS. A square block of data was captured and cortex filters at various directions and radial bands were applied to filterout the required frequency components. The output of the filters were used to compute average energy and magtitude deviation as texture features in the block. We repeated this procedure for the subsequent blocks of data. Hence we obtained a set of feature images. The obtained feature images were then integrated with minimum distance classifier for supervised and k-means algorithm for unsupervised classification. We demontrated the performance of our approach by experiments on real world scence images from camera, Brodatz's album and satellite sensors. Comparison with Haralick's gray-level co-occurence matrix(GLCM) and discrete wavelet frame(DWF) based approaches show the superiority of our method.

1 Introduction

Many earth observation systems provide us with plenty of images of our planet. Together with an increasing resolution, the amount of numerical data drastically increases including the complexity of individual images. Therefore, means for automatic extraction of useful information from the steadily growing archives become necessary. Information in this kind of images is mainly contained in the multi-variate statistics of the different image channels due to the different reflectivities in the spectral bands of electromagnetic radiation. The use of spectral features for image classification is one of the standard techniques widely used in remote sensing [1]. However, spectral classification often fails with the changes in illumination conditions or non-uniform illuminations. Furthermore, if spatial context is needed to identify particular cover types, such as 'urban' or 'fields', spectral properties do not provide robust representation whereas texture is an invaluable feature to take into account. But due to its randomness and the spatial continuity in the local and global scale, it is quite difficult to give a universal definition of texture. According to Sklansky [2], " A region in an image has a constant texture if a set of local statistics or other properties of the picture are constant, slowly varying or approximately periodic".

Over the past three decades, a large number of approaches, mainly categorized into statistical and signal processing methods, have been developed. Statistical methods include Gray-level co-occurence matrix(GLCM)[3, 4, 5, 6], Markov random fields model [7, 8], fractal geometry [9, 10, 11]. Signal processing methods include various spatial/frequency domain filtering mechanisms [12, 14, 15, 16, 17, 13, 18, 20, 19, 23] based on Gaussian, Laplacian, wavelet(Gabor), and spatial moments. However, texture features still have not been established as standard tools for remote sensing image interpretation. In this paper we, therefore, propose a block processing concept using popular cortex transform and demonstrated its performance in the remote sensing, normal camera, and standard Brodatz texture images.

The contribution is structured as follows:

1. Develop a block processing system, where cortex filters were applied within a sliding block centered around a pixel rather than over entire image fre-

*Department of Information Engineering, Nagoya University, Furo-cho, Chikusa-ku Nagoya 464-8603, Aichi, Japan

**Department of Computer Science and Information Technology, Islamic University of Technology Board Bazar, Gazipur-1704, Bangladesh

quency plane.

2. Reduction of feature space dimensions by experimental selection of the block size which automatically fixes the required scales based on octave spacing.

3. HVS based features appear suitable to the well known classifiers like minimum distance and k-means algorithm.

In our approach, we applied cortex filters within a square block of data. Average energy and magnitude deviation computed on the filtered images are regarded as texture features. Moving the window throughout the entire image and calculating texture features for each obtain a set of feature images. The feature set is subsequently classified using above mentioned classifiers.

In section 2 we briefly explain cortex transform with associated filters. Section 3 presents detail classification system, in which we explain block-based feature computation technique. In section 4, we present the results and comparative study with GLCM and DWF based approaches. Finally we discuss the work in section 5 and conclude it through section 6.

2 Cortex Transform

The cortex transform [17] decomposes an input image into a set of sub-images according to the behavior of simple cells of HVS. The band pass nature of the simple cells is modelled by the cortex filter, which is a product of two gaussian functions in the frequency domain, namely radial band and orientation filters with a radial and orientation bandwidth of 1 octave and 45 degrees respectively. In polar cordinate system, they are represented as follows.

Radial band filter:

$$f(r) = \frac{1}{\sqrt{2\pi}\sigma_r} \exp\{-\frac{(r - m_r)^2}{2{\sigma_r}^2}\} \qquad (1)$$

Orientation filter:

$$g(\theta) = \frac{1}{\sqrt{2\pi}\sigma_\theta} \exp\{\frac{-(\theta - m_\theta)^2}{2\sigma_\theta^2}\} \qquad (2)$$

Cortex filter:

$$C(r,\theta) = f(r)g(\theta) \qquad (3)$$

where

$$m_r = \mathrm{Int}[\frac{r_1 + r_2}{2}], \qquad (4)$$

$$\sigma_r = \sqrt{-\frac{(r_1 - m_r)^2}{2\ln(R_r)}} \qquad (5)$$

$$R_r = \frac{f(r_1)}{f(m_r)} \qquad (6)$$

$$m_\theta = (\text{indices})\frac{\pi}{4} + \frac{\pi}{8}, \qquad (7)$$

$$\sigma_\theta = \sqrt{\frac{-(\frac{\pi}{8})^2}{2\ln(R_\theta)}} \qquad (8)$$

$$R_\theta = \frac{g(\frac{\pi}{8} + m_\theta)}{g(m_\theta)} \qquad (9)$$

Here $Int[.]$ is a function to compute the integer value of the argument, r and θ are the frequency variables and r_1 , r_2 are the filter corner frequencies respectively. m_r, m_θ are means, σ_r, σ_θ are standard deviations, and R_r, R_θ are ratio parameters of the Gaussians respectively. 'Indices' are integer values (0,1,2,3) used to obtain center frequencies of the orientàtion filters. The frequency spectrum of a sample radial band , orientation, and cortex filter are shown in Fig.1. The detail computation of the various filter parameters will be found in [17] [21].

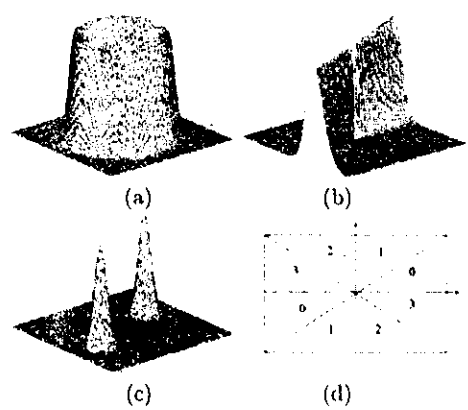

Figure 1: The frequency spectrum of a sample (a) Radial band filter, (b) Orientation filter, (c) Cortex filter, and (d) Indices for orientation filters

3 Classification system

A detail classification system consists of the following sub-sections.

3.1 Filter kernel generation

Filter kernel in the frequency domain, as shown in table 1, is generated using Eq. (1)-(9). The various steps are summarized as follows:

1. Select the size of the kernel equal to sliding window size i.e, 16x16 in our case.

2. Choose an initial radial frequency, f_{int} (2 in our case) and determine number of frequency fairs within the window following octave rule. For each pair compute also the means and standard deviations using Eq. (4)-(9) for a chosen value of R_r or R_θ between 0.01 to 0.03.

3. Calculate frequency variables r and θ and also compute $f(r)$ and $g(\theta)$ for $r_i \leq r \leq r_j$ and $\theta_m \leq \theta \leq \theta_n$, where i, j indicate the lower and upper radial frequency indices and m, n are orientation indices respectively.

4. Compute cortex filter as $C(r,\theta) = f(r)g(\theta)$.

Table 1: Filter Kernel for a sample (8x8) window, where R_r or R_θ is 0.01, $r_1 = f_{int} = 2, r_2 = 4$, and $\theta_1 = 0, \theta_2 = \frac{\pi}{4}$.

v, u	-4	-3	-2	-1	0	1	2	3
4	0	0	0	0	0	0	0	0
3	0	0	0	0	0	0	0	0
2	0	0	0	0	0	0	.220	0
1	0	0	0	0	0	.218	2.848	0
0	.038	0	0	0	0	0	.038	0
-1	2.848	.218	0	0	0	0	0	0
-2	.220	0	0	0	0	0	0	0
-3	0	0	0	0	0	0	0	0

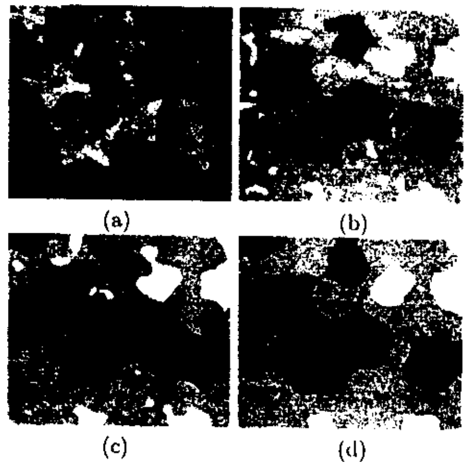

Figure 2: Effect of window sizes on class boundary, (a) Original flower-1 image (256x256), (b), (c), and (d) Classified images by our BPA approach for window sizes (8x8), (16x16), and (32x32).

Table 2: Orientation filters per radial band.

Range	Angle
$R_1 \leq r \leq R_2$, where	$0^o \leq \theta \leq 45^o$
$R_1 = 2, 4$ and $R_2 = 4, 8$	$45^o \leq \theta \leq 90^o$
cycles per pixel	$90^o \leq \theta \leq 135^o$
	$135^o \leq \theta \leq 180^o$

3.2 Window selection

In our analysis, window size is very important as it determines the feature space dimension and scales. For the segmentation study, the window size should include pixels from a single texture class and usually the smaller the size, the better is the performance. On the other hand, a reasonably larger size is expected for better texture characterization. As our present efforts, the window size is determined as 16x16 based on a boundary verification experiment over a number of images. The principle is to compromise between the stability and resolution. Figure 2 shows how various window sizes affect the class boundaries. However automatic selection of window size is an important issue yet to be solved.

3.3 Filter selection criterion

In our implementation, octave scale is used during filter selection within the image block mentioned above. This is justified by the radial frequency bandwidth of the simple cells in the visual cortex of HVS. According to this scale, number of cortex filters required is

$$NCF = 4\log_2[(N/2)/f_{int}] \tag{10}$$

where N represents a square block size and f_{int} is the initial radial frequency. For a square window of size (16x16), the total number of filters can be calculated from table 2.

If we choose an initial radius of 2 units, the number of cortex filter are 8. Again to cover the central (low frequency) and outermost regions of the block two Gaussian isotropic filters are used. Implementation shows that these two filters help to extract relatively coarser and finer textural regions. So the total number of filters becomes (NCF+2) i.e., 10 in our example. Observed that the logarithmic term in the above equation represents number of scales, which is three (3) for our (16x16) block with unit lowest radial frequency.

3.4 Feature image formation

Feature images are computed based on the average energy and magnitude deviation of the filtered images computed over a square block with center $(x_o, y_o$.

$$E_{ij}(x_0, y_0) = \frac{1}{N^2}\sum_{x=0}^{N-1}\sum_{y=0}^{N-1}|F_{ij}(x,y)|^2 \qquad (11)$$

$$MD_{ij}(x_0, y_0) = \sqrt{\frac{1}{N^2}\sum_{x=0}^{N-1}\sum_{y=0}^{N-1}(|F_{ij}(x,y)| - \mu_{|F_{ij}|})^2} \qquad (12)$$

,where N^2 represents number of pixels within a window and $F_{ij}(x, y)$ is the filtered image, and $\mu_{|F_{ij}|}$ its mean magnitude in the i-th scale and j-th orientation.

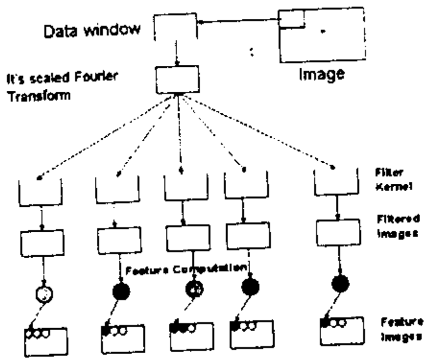

Figure 3: Flow diagram for feature image formation

A square block of data is windowed from the original image and is transformed by using popular Fourier transformation technique. Various frequency components characterizing radial and orientation properties of texture in the block are filtered out in the frequency domain by using cortex filters. Then average energy and magnitude deviation corresponding to each filtered magnitude response are calculated as texture features. Thus the feature values obtained from the various filters are stored as the first pixel value of a set of 2D arrays. Now next block of data is selected through appropriate horizontal shifting of the window. Hence the calculated feature values are stored as the second pixel of the previous set of arrays. In this way, through horizontal and vertical shifting of the window over the original image and putting the calculated features as various pixels of the arrays, a set of feature images are generated. Figure 3 shows the block diagram of the technique described.

3.5 Feature image integration

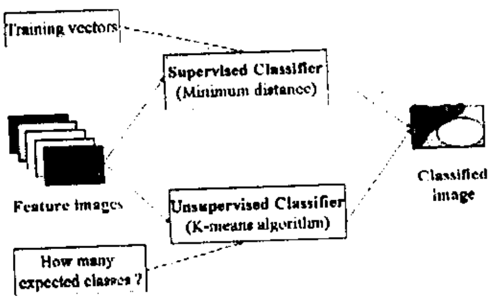

Figure 4: Supervised and unsupervised classification

In the supervised classification, visual samples are used for representative class vectors formation. In fact manual identification of the true classes is essential in supervised method. However, the same technique as the texture feature computation is adopted in the training phase for training vectors formation. Some samples (maximum 3) from each expected class of the input image are visually selected as true samples. We then computed and averaged out sample-training vectors in each class to obtain individual class representative vector. Feature images and the representative vectors calculated above are inputted to the minimum distance classifier. Classifier computes all euclidean distances between an unknown vector to the all known training vectors. We then label the concerned pixel based on the minimum distance calculated from the above distances. The same procedure is exercised until the labeling of entire image pixels is completed. This is how we obtain the classified image.

K-means algorithm is used for unsupervised classification. Instead of visual samples, the user just provides two inputs to the classifier. 1) Number of major classes k, in the input image. 2) A set of feature images previously generated. The classifier iteratively modifies the randomly selected mean vectors until an error criterion is satisfied. Of course the population in each class grows based on the euclidean distances between unknown vector to randomly selected mean vectors. Figure 4 shows a simple block diagram of our classification method.

4 Results and comparative study

4.1 Results

Our algorithm is tested over a group of 20 images from camera, satellite sensors and Brodatz's album and appears to be promising with respect to classification accuracy (see section 4.2). Our block processing operation has also flexibility in computational time depending on the extent (number of pixels) through which the sliding window is shifted. Approximately 10 minutes for 1 pixel, 2.5 minutes for 2 pixels, 0.625 minutes for 4 pixels shifting for an image of size 256 x 256 using Pentium (P-III, 800 MHz, 128MB RAM) machine in the LINUX environment. However, single pixel shifting produces best boundary, whereas blocking effects come into picture gradually for multi-pixels shifting. Circular window may be used to reduce blocking effect with the gain of computational efficiency. Figures 5 and 6 show a set of original and classified images obtained from supervised and unsupervised methods through 1 pixel shifting of the block. The original images have the following description.

1. Valley water image (256x256), Camera image,
2. Oily water (256x256), RADARSAT image,
3. Osaka-jetty area (256x256), LANDSAT image,
4. Shanghai river (256x256), LANDSAT image,
5. Fired mountain (256x256), SPOT AVHRR image,
6. Mosaic-1(128X128), Brodatz's album,
7. Mosaic-2 (256x256), Brodatz's album,
8. Mosaic-3(256X256), Brodatz's album,
9. Scene image (256x256), Camera image,
10. Flower-2 image (256x256), Camera image.

From the valley water image, it is observed that our algorithm can distinguish between land and water very clearly. Satellite images (oily water, Osaka-jetty, shanghai river, fired mountain) are also classified into constituent classes very well. It is worthy to mention that our approach can distinguish between severely oily water from less oily or non-oily part of the oily water image. In the Osaka-jetty image, we observe that BPA approach distinguishes the jetty-working area from water and other part of the soil.

(a) (b) (c)

Figure 5: (a) Original image, Classified images (b)supervised, (c) unsupervised

Furthermore it can isolate fire area from the normal ground in case fired mountain image. However, smoke region of this image is mis-classified as fire. In shanghai river image, we see the newly cultivated area (grey or dark region in the central part of the image) is separated from the rest of the soil and river. Standard texture (mosaic) images are also well classified except a minor boundary problem.

4.2 .Comparative study

We have performed comparative study in two aspects.

In the first case, a visual comparison between supervised and unsupervised classification results is shown in Figs. 5, 6 based on our BPA features. Results show a very competitive outcome without remarkable distinction of overall performance between the two.

In the second case, visual as well as confusion matrix analysis is performed between our BPA with GLCM and DWF based approachs for supervised classification. Figure 7 shows that our BPA approach performs well in terms of classification accuracy and noise suppresion in all types images. Specially the natu-

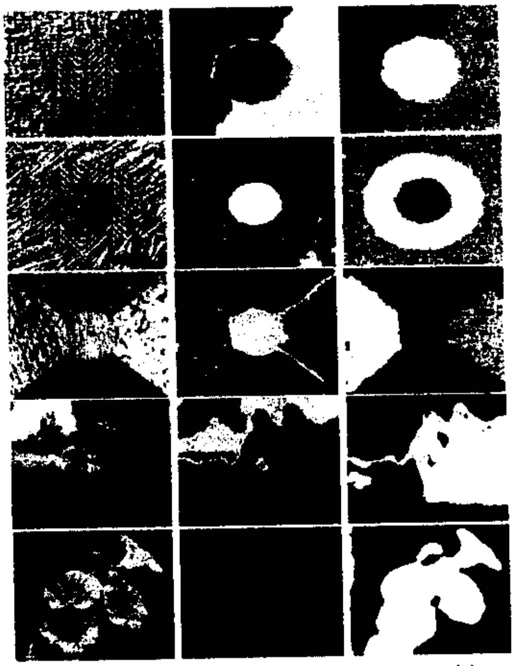

(a) (b) (c)

Figure 6: (a) Original image, Classified images(b)supervised, (c) unsupervised

ral (flowers, valley water, and scene) images are well classified with respect to accuracy and boundary extraction. Our BPA clearly extracts the cloud regions from the scene image, where both the GLCM and DWF based approaches fail. However, DWF based approach performs better in case of mosaic textures both in terms of noise suppression and boundary extraction. While GLCM approach produces smoother boundary at the cost noises.

4.2.1 Gray-level co-occurence matrix approach

Gray-level co-occurrence matrix is a two dimensional matrix of joint probabilities $P_{d,r}(i,j)$ between pairs of pixels, separated by a distance, d, in a given direction, r. It is popular in texture description and is based on the repeated occurrences of some gray level configuration in the texture. This configuration varies rapidly with distance in fine textures, slowly in coarse textures [3]. Finding texture features from gray-level co-occurrence matrix for texture analysis in this experiment are based on the following well known features:

Table 3: Confusion matrix for the classified oily-water image obtained from BPA.

	$C1$	$C2$	$C3$	$C4$	$Total$	$ICA(\%)$
C1	512	0	0	0	512	100.0
C2	0	512	0	0	512	100.0
C3	0	0	512	0	512	100.0
C4	0	0	0	512	512	100.0
Total	512	512	512	512		

Overall accuracy(OA) is 100.0%

$$Energy = \sum_i \sum_j P_{d,r}^2(i,j) \tag{13}$$

$$Entropy = -\sum_i \sum_j P_{d,r}(i,j)\log(P_{d,r}(i,j)) \tag{14}$$

$$Contrast = \sum_i \sum_j (i-j)^2 P_{d,r}(i,j) \tag{15}$$

$$Homogeneity = \sum_i \sum_j \frac{P_{d,r}(i,j)}{1+|i-j|} \tag{16}$$

We used co-occurrence lengths of 1 and $\sqrt{2}$ pixels to calculate above features. A linear gray-scale quantization to 40 levels is also performed to limit the size of the co-occurrence matrix and to save computational time.

Table 4: Confusion matrix for the classified oily-water image obtained from GLCM approach.

	$C1$	$C2$	$C3$	$C4$	$Total$	$ICA(\%)$
C1	99	16	41	356	512	19.34
C2	242	88	0	182	512	17.19
C3	62	0	450	0	512	87.89
C4	0	0	0	512	512	100.0
Total	512	512	512	512		

Overall accuracy(OA) is 56.10 %

Table 5: Confusion matrix for the classified oily-water image obtained from DWF based approach.

	$C1$	$C2$	$C3$	$C4$	$Total$	$ICA(\%)$
C1	150	240	103	19	512	29.30
C2	0	388	0	124	512	75.78
C3	0	0	512	0	512	100
C4	0	76	0	436	512	85.16
Total	512	512	512	512		

Overall accuracy(OA) is 72.56 %

4.2.2 Wavelet Frame Decomposition(WFD) based Method

Discrete wavelet transform is an elegant tool for multiresolution texture analysis. However down-sampling during decomposition does not properly characterize the shift invariance properties of texture. Therefore discrete wavelet frame(DWF)[24] may be used. We used 1D Dubechies-4 wavelet filter [25] to decompose the signal without downsampling. So the sub-bands have the same size as the original image. Four levels of decomposition for 256x256 images is used in our studies. The average energy of the high frequency subbands are computed at every pixel over a sliding window. These sub-band energy is regarded as texture features. We used a square window of size 13x13 for the above implementation.

$$E_s(x_0, y_0) = \frac{1}{N^2}\sum_{x=1}^{N}\sum_{y=1}^{N}|W_s(x,y)| \qquad (17)$$

Here N is the window size with center (x_0, y_0), s indicates the number of decomposition scales and $W_s(x,y)$ is the pixel transform coefficient value. Thus a set of energy images are constructed corresponding to subband images. These are directly applied to minimum distance classifier for supervised texture classification.

4.2.3 Confusion matrix analysis

Confusion matrix analysis is performed on the classified images obtained from supervised method. As the true boundaries of expected texture classes are unknown, we did not use the entire classified image for the above analysis. Instead, we used some carefully selected samples (by the expert user) for the error matrix formation. The labels of the user fixed pixels compared with the same positioned classifier estimated pixel labels to construct confusion matrices, whose diagonal entries reflect the accuracy of classification. We then compute individual (ICA) and overall classification accuracy (OA) using Eq. 18 and Eq.19.

$$ICA = \frac{C_{ii}}{\sum_{j=1}^{n} C_{ij}} \qquad (18)$$

$$OA = \frac{\sum_{i=1}^{n} C_{ii}}{\sum_{i=1}^{n}\sum_{j=1}^{n} C_{ij}} \qquad (19)$$

where C_{ii}'s $(i = j)$ are entries for correct classification and C_{ij} 's $(i \neq j)$ are misclassified pixels in the window being considered. Tables 3, 4, and 5 show the error matrices computed from the classified oily water images, obtain from our BPA, GLCM, and DWF based approaches. The diagonal entries of the matrices indicate the strength of our BPA.

In order to demonstrate the performance of our approach, we computed overall classification accuracy (OA) over seven images from different categories (natural, mosaic, remotely sensed). Results indicate the superiority of our approach consistently with a gain of average overall accuracy of 24.26 % and 20.66% compared to GLCM and DWF based approaches respectively. Figure 7 7 and Table 6 confirm our claims subjectively and objectively.

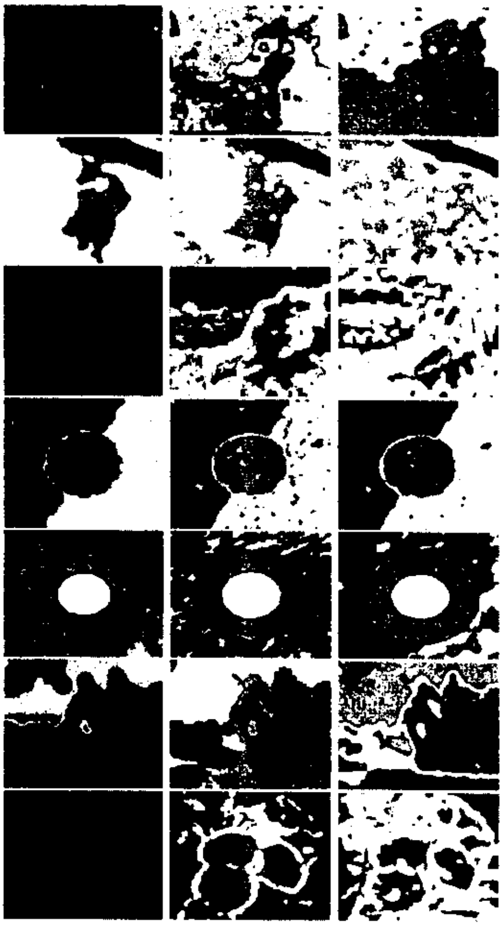

(a) (b) (c)

Figure 7: Classified images(a) Our BPA (b)GLCM approach, and (c) DWF based method

Table 6: Comparison of overall class accuracy between BPA and GLCM approach.

Images	Number of sample pixels	(Supervised) overall accuracy,OA (%) BPA	GLCM	DWF
Natural Scene	3840	92.03	65.70	78.51
Mosaic-1	12288	99.51	96.34	99.21
Mosaic-2	2048	92.85	90.43	99.74
Oily water	2048	100.0	56.10	72.56
Shanghai river	2304	95.57	85.37	70.49
valley water	1536	100.0	80.534	40.43
Flower2	1536	100.0	76.758	74.15
Average OA (%)		A: 97.58	B: 73.32	C: 76.92
Accuracy(OA) gain(%)		A-B=24.26, A-C=20.66		

5 Discussion

In our implementation, we select a window size as 16x16 based on the experiment to compromise between resolution and stability. However, the algorithm may be modified for automatic window size selection based on image frequency analysis. Autocorrelation width may be used to determine the size (lowest and highest) of the texture primitive, that is to obtain the window size especially for regular textured images.

During filter kernel generation, initial radial frequency was chosen to be 2 or 4 units away from the lowest frequency content. Filter pass band controlling parameter ratio, $R_r or R_\theta$ is observed to be suitable between 0.01-0.03 for various types of images. Phase information of images is also important factor to consider as it can contribute to the texture analysis [22]. Again we did not use the overlapping of filter kernels within a data block. However, appropriate overlapping can produce more uniform coverage of the frequency plane. Although in general most of the signal energy is concentrated in the lower frequency ranges, our block based approach discards high frequency information to an extent. Appropriate block size might encompass sufficient filters necessay to extract required frequency information.

6 Conclusion

A novel block processing approach for dealing with the image texture is proposed here for classification of images. Our algorithm reduces feature space through applying filters within small blocks fixed experimentally. This is why we did not use optimal filter selection scheme. We also relaxed applying post-filtering transformation as our block based features appear to be suitable for texture characterization.

Comparison with the GLCM and DWF based methods show the superiority of our approach in terms of classification accuracy over various types of images specially natural images as mentioned. It is observed that both GLCM and DWF based methods failed to classify natural images despite their better performances in terms of boundary extraction of mosaic textures.

Moreover, our block processing approach provides noise smoothing automatically. However, phase information and non-uniform illuminations were not considered in our study. So automatic window size selection, inclusion of phase information, and analysis in the noisy and varying illuminating environment are open for future study.

Acknowledgements

We express gratitude to Dr. R. K. Banik of the environmental medicine institute of Nagoya university for his valuable comments during manuscript preparation. We also thank Mr. T. Mizuno for Latex report software installation and settings. Parts of this work have been supported by the Hori Science Information Foundation, Japan.

References

[1] J. B. Campbell, *Introduction to remote sensing*, Taylor and francis, 2nd edition, 1996.

[2] Anil K. Jain and farshid Farrokhnia, "Unsupervised Texture segmentation using Gabor Filters," *Pattern Recognition*, vol. 24, no. 12, pp. 1167-1186, May 1991.

[3] R.M. Haralick, K. Shanmugam and I. Dinstein, "Textural features for Image classifications," *IEEE Trans. Syst. Man. Cybern.*, Vol.3, pp. 610-621, 1973.

[4] J. Sklansky, " Image Segmentation and feature extraction," *IEEE Trans. Syst. Man. Cybern.*, vol. 8, pp. 237-248, 1978.

[5] C.C. Gotlieb and H.E. Kreyszig, " Texture descriptors based Co-occurance Matrices," *Computer Vision Graphics Image Process.*, Vol. 51, pp. 70-86, 1990.

[6] Chung-Ming Wu and Yung-Chang Chen, "Statistical feature matrix for texture analysis," *CVGIP: Graphical Model and Image Processing*, vol. 54, no. 5, pp. 407-419, Sep. 1992.

[7] R. Chellappa and S. Chatterjee, "Classification of Texture Using Gaussian Markov Random Fields," *IEEE Transactions on Acoustic, Speech, and Signal Processing*, ASSP-33, pp.959-963,1985.

[8] G. C. Cross and A. K. Jain, "Markov Random Field Texture Models," IEEE Transaction on Pattern Analysis and Machine Intelligence, PAMI-5, pp. 25-39, 1983.

[9] A. Pentland, " Fractal-based description of natural scenes," *IEEE Transaction on Pattern Analysis and Machine Intelligence*, PAMI-9, pp.661-674, 1984.

[10] J. M. Keller, S. Chen, and R. M. Crownover, "Texture Description and Segmentation through Fractal Geometry," *Computer Vision, Graphics, and Image Processing*, Vol. 45, pp. 150-166, 1989.

[11] B. J. Super and A. C. Bovik, "Localized Measurement of Image fractal Dimension Using Gabor Filters," *Journal of Visual Communication and image Representation*, Vol.2, pp. 114-128, 1991.

[12] Dennis Dunn and William E. Higgins, "Optimal Gabor Filters for texture segmentation," *IEEE Trans. Image Processing*, Vol.4, no.7, pp.947-963, July 1995.

[13] M. R. Turner, "Texture Discrimination by Gabor Functions," *Biological Cybernetics*, Vol.55, pp.71-82, 1986.

[14] Chun S. Lu, Pau C. Chung and Chih F. Chen, "Unsupervised Texture segmentation via Wavelet Transform," *Pattern Recognition*, vol. 30, no. 5, pp. 729-742, 1997.

[15] Zhu, C., and X. Yang, " Study of Remote Sensing Image Texture Analysis and Classification using wavelet," *International Journal of Remote Sensing*, vol.13, pp 3167-3187, 1998.

[16] Pasaresi, M., "Texture Analysis for Urban Pattern Recognition using Fine-resolution Panchromatic Satellite Imagery," *Geographical and Environmental Modelling*, vol. 4, no.1, pp.43-63, 2000.

[17] C. Goresnic and S.R. Rotman, "Texture Classification Using the Cortex Transform," *CVGIP: Graphical Models and Image Process.*, vol.54, no.4, pp. 329-339, 1992.

[18] J. Portilla and E. P. Simoncelli, "Texture Modelling and Synthesis using Joint Statistics of Complex Wavelet Coefficients," *Proceedings of the IEEE workshop on Statistical and Computational Theories of Vision*, Fort Collins, CO, June 1999.

[19] L. Balmelli and A. Mojsilovic, " Wavelet Domain Features for Texture Description, Classification and Replicability Analysis," *Proceedings of IEEE International Conference on Image Processing (ICIP)*, Vol. 4, pp.440-444, October 1999.

[20] P. Scheunders, "A multivalued image wavelet representation based on multiscale fundamental forms," *IEEE Transaction on Image processing*, to appear in 2001.

[21] M.K. Bashar, B.K. Mohan, R.K. Shevgaonkar, N. Ohnishi, "Unsupervised Texture Classification of Images using Cortex Filters," *Proceedings of the 5th Asian Conference on Computer Vision*, Vol.II, pp.828-833, January 22-25, 2002.

[22] H. Tanaka, Y. Yoshida, K. Fukami, and H. Nakano, "Texture Segmentation using Amplitude and Phase Information of Gabor Filters," *IEICE Transactions D-II*, Vol. J84-D-II, pp.2565-2576, December 2001.

[23] P. Scheunders and S. De Bacher, "Multispectral Image Fusion and Merging using Multi-scale Fundamental Forms," *Proceedings of the IEEE International Conference on Image Processing*, Greece, October 7-10, 2001.

[24] M. Unser, "Texture classification and segmentation using wavelet frames," *IEEE Trans. Image Proc.*, Vol. 4, pp. 1549-1560, 1995.

[25] I. Daubechies, " Orthogonal based of compactly supported wavelets," *Commun. Pure Appl. Math.*, Vol.41, pp.909-966, 1988.